Int. J. Electrochem. Sci., 7 **(2012)** 9550 - 9559

International Journal of
ELECTROCHEMICAL
SCIENCE
www.electrochemsci.org

Cerium Oxides as Oxygen Reduction Catalysts for Lithium-Air Batteries

Xiujing Lin, Lan Zhou, Tao Huang, Aishui Yu[*]

Department of Chemistry, Shanghai Key Laboratory of Molecular Catalysis and Innovative Materials, Institute of New Energy, Fudan University, Shanghai 200438, China
[*]E-mail: asyu@fudan.edu.cn

Received: 21 August 2012 / *Accepted:* 10 September 2012 / *Published:* 1 October 2012

In this work, CeO_2 of different morphologies were fabricated and used as the cathode catalysts for oxygen reduction reaction (ORR) of lithium-air batteries. Due to its easy shift between reduced and oxidized states, the discharge potential of lithium-air battery using CeO_2 as the cathode catalyst is nearly 0.1 V higher than that of the cathodes without a catalyst at the current density of 0.05 mA cm^{-2}. Simultaneously, it shows a higher capacity of 2128 mAh g^{-1}. The morphologies effect on the discharging performance is further investigated. CeO_2 nano-particles (NP-CeO_2) with a high surface area of 63.1 m^2 g^{-1} exhibits the superior capacity. Not only surface area but also crystal structure of cerium oxides play a great role on their electro-catalytic performance in lithium-air batteries.

Keywords: Lithium-air battery, Electrocatalysis, Oxygen reduction reaction (ORR), CeO_2

1. INTRODUCTION

Lithium-air battery has captured considerate attention since its first reported by Abraham and Jiang [1]. It delivers a theoretical specific capacity as high as 3860 mAh g^{-1}, which exhibits significant advantages over electrical storage devices in hybrid electric vehicles (HEVs) and electric vehicles (EVs) [2, 3]. In general, a Lithium-air battery consists of a lithium anode, nonaqueous electrolyte and an air cathode, which can absorbs oxygen from the environment. The electrochemical reactions are involved when it is discharged:

$$4Li+O_2 \rightarrow 2Li_2O \qquad (E^{\theta}= 2.9\ V)$$

$$2Li+O_2 \rightarrow Li_2O_2 \qquad (E^{\theta}= 3.1\ V)$$

However, much work still needs to be done to make it for practical use. The foremost challenge is the existence of huge polarization during the oxygen reduction reaction (ORR), which has a close relationship with the consequent oxygen evolution reaction (OER). Much work has reported to lessen the polarization and improve the capacity by the addition of catalysts, such as MnO_2 [4, 5], α-MnO_2/Pd [6], manganese oxide with "card-house-shaped" [7], titanium containing γ-MnO_2 [8], MnO_2 nanoflakes [9], PtAu [10], Co_3O_4@Ni [11], MoN/NGS [12], Co_2MnO_4 [13], $CoMn_2O_4$ [14], $Ag_2Mn_8O_{16}$ [15], $La_{0.8}Sr_{0.2}MnO_3$ [16], $Co(phen)_2$/C [17] and so on.

Another critical challenge is the low oxygen solubility in the nonaqueous electrolyte [18, 19]. According to the liquid-solid model of "two-phase reaction zone" proposed by Jeffrey Read et al [20], oxygen reduction occurs between electrolyte and carbon interface. The air cathode is wetted by nonaqueous electrolyte. However, low oxygen solubility in the nonaqueous electrolyte imposes restrictions on power density. To make it worse, Li_2O and Li_2O_2 deposit on the surface of an air cathode and block the access of oxygen to catalytic sites. Therefore, a catalyst serving as "oxygen buffer" will relieve oxygen insufficiency. Ceria (CeO_2) is widely regarded as a key catalyst candidate for its easy shift between reduced and oxidized states as a result of change in gas phase oxygen concentration [21]. It could be expounded briefly as follows:

$$CeO_2 \leftrightarrow CeO_{2-x} + (x/2)\ O_2 \quad (0 \leq x \leq 0.5) \qquad (1)$$

This enables it to provide oxygen under lean conditions and remove it under rich conditions [22]. Furthermore, CeO_2 can retain its face cubic structure even when severe deviation from its stoichiometry and the oxygen vacancy could provide sites for catalytic activity [23].

In this work, we synthesized CeO_2 of different morphologies by coprecipitation and hydrothermal method, respectively. Lastly, lithium-air batteries catalyzed by the as-synthesized catalysts were constructed and tested in order to investigate their catalytic activity on ORR.

2. EXPERIMENTAL

2.1. Synthesis of catalysts

CeO_2 nano-particles (NP-CeO_2) were prepared by adding 10 ml aqueous ammonia (25-28%，Taicang Zhitang Chemical Industry Co., Ltd) to 0.1 M $CeCl_3$ (99%, Sinopharm Chemical Reagent Co.,Ltd) methanol solution under vigorous stirring. After precipitation, the solid was dried at 293 K for 12 h and further calcined at 673 K in air for 4 h.

To obtain CeO_2 spheres (S-CeO_2), 0.25 M $Ce(NO_3)_3$ (99.0%, Sinopharm Chemical Reagent Co.,Ltd) and an appropriate amount of $Na_3PO_4 \cdot 6H_2O$ (99.0%, Sinopharm Chemical Reagent Co., Ltd, the molar ratio of PO_4^{3-} to Ce^{3+} was remained at 5%) were dissolved in 30 and 10 mL deionized water, respectively. Then, the two solutions mixed. After 30 min of magnetic stirring, the homogenous solution was transferred into the 50 mL Teflon-lined autoclave and kept at 493 K for 12 h. After that,

the fresh precipitates were collected by centrifugation and washed several times with distilled water and absolute ethanol, and dried in the air at 333 K.

CeO_2 octahedra (O-CeO_2) were synthesized by dissolving 1 mmol $CeCl_3 \cdot 7H_2O$ (99.0%, Sinopharm Chemical Reagent Co., Ltd) and 10 mmol $CO(NH_2)_2$ in 50 mL deionized water. Then, 100 mL deionized water was added to the solution and kept stirring for 10 min. Subsequently, the homogenous solution was transferred into the 50 mL Teflon-lined autoclave and heated for 4 h at 453 K. After that, the precipitates were collected by centrifugation and washed with distilled water and absolute ethanol, and dried at 333 K in the air.

2.2. Characterization

The as-synthesized catalysts were characterized by X-ray powder diffraction on a Bruker D8 Advance X-ray diffractometer using Cu Kα radiation at a scan rate of 5 deg min^{-1}. The morphologies were observed by scanning electron microscopy (SEM, Hitachi, FE-SEM S-4800A) and transmission electron microscope (TEM, JEM -2100F). Brunauer-Emmet-Teller (BET) surface areas of these catalysts were measured on a Micromeritics Tristar 3000.

2.3. Electrochemical measurement

Cathode was prepared by casting a mixture of Super P, catalysts above and PVDF with a total weight ratio of 2:1:1.5 onto a separator (Celgard 3500). The resultant air cathode sheet was punched into small disks with a diameter of 12 mm and dried at 80℃ for 12 h. For charge/discharge tests, lithium-air batteries were constructed in an argon atmosphere glove box ($H_2O \leq 10$ ppm) by use of Swagelok batteries with an air window of 78.5 mm^2. They were assembled by stacking a Li foil, a Celgard 3500 membrane, different air cathodes and Al mesh as the current collector. The nonaqueous electrolyte consisted of 1 M $LiPF_6$ in propylene carbonate (PC)/dimethyl carbonate (DMC) at a ratio of 1:1 w/w. Discharge/charge measurements were carried out on a Land cycler (Wuhan Jinnuo Electronic Co. Ltd.) in a voltage range of 2.0-4.5 V vs. Li^+/Li at various discharge current densities.

Before each test, there was a 2 h rest for the batteries in order to reach equilibrium of oxygen between the ambient environment and the cathode. All the tests were carried out at room temperature.

3. RESULTS AND DISCUSSION

3.1. Structure and morphology characterization

The XRD patterns of NP-CeO_2 are shown in Fig. 1, which are in good agreement with the literature [21]. The characteristic sharp diffraction peaks of NP-CeO_2 indicate the presence of crystalline phase. As is shown in Fig. 2a, the NP-CeO_2 sample appears to be a combination of nano-particles, which aggregate with each other to form the film-like morphology.

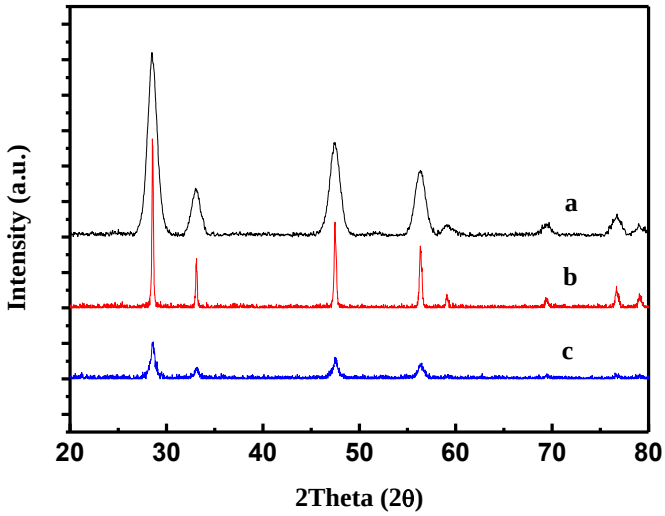

Figure 1. XRD patterns of (a) NP-CeO_2, (b) O-CeO_2 and (c) S-CeO_2.

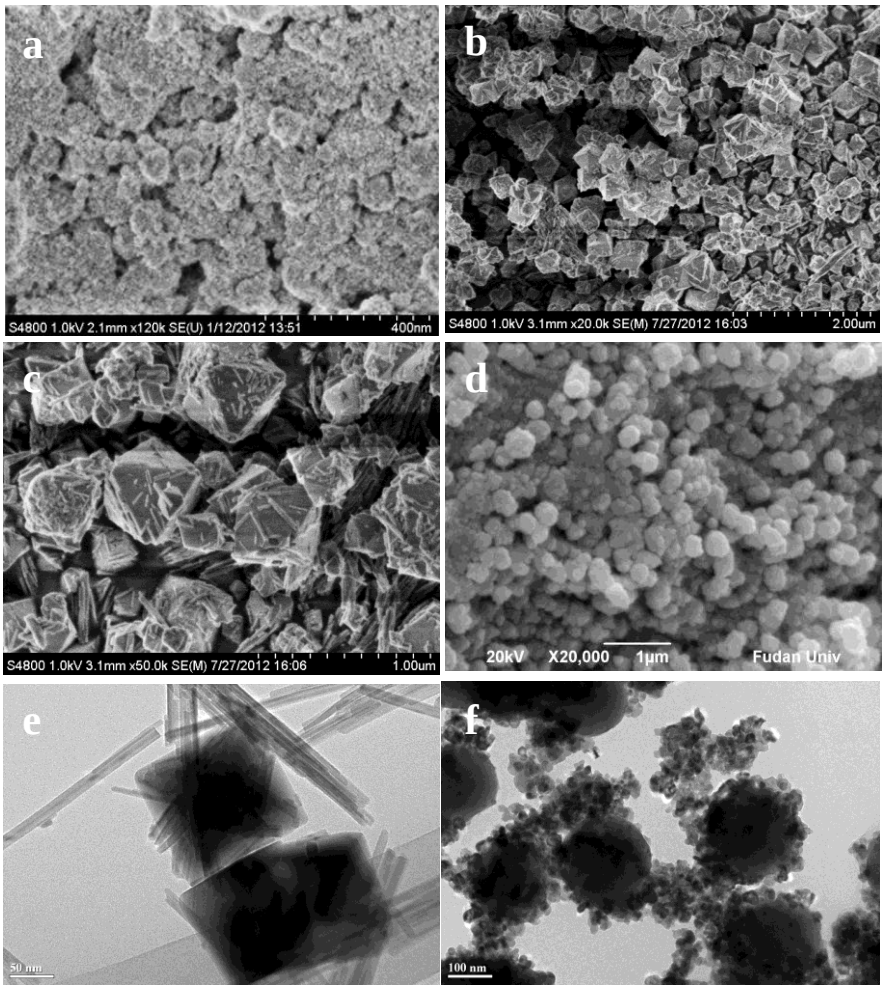

Figure 2. SEM images of (a) NP-CeO_2, (b, c) O-CeO_2 and (d) S-CeO_2. TEM images of (e) O-CeO_2 and (b) S-CeO_2.

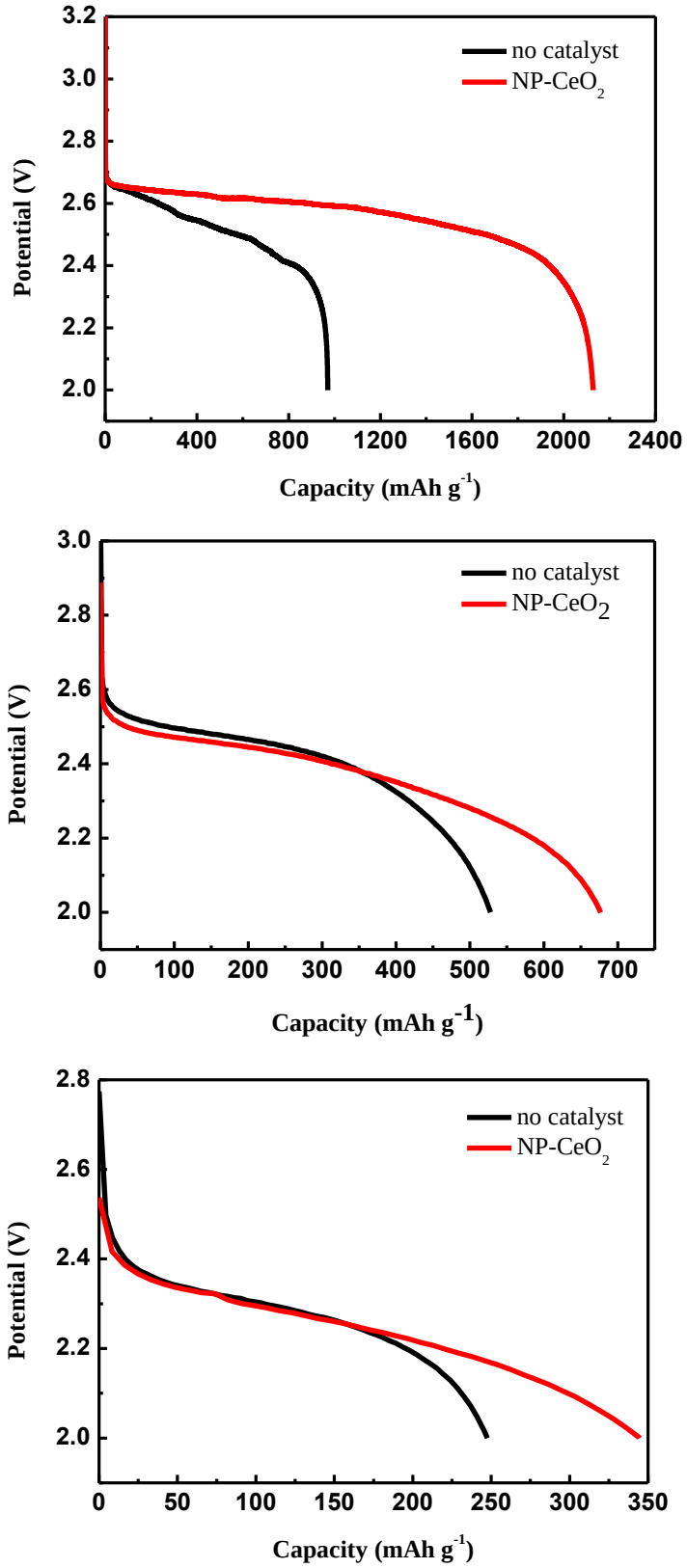

Figure 3. Discharge characteristic of lithium-air batteries at various current densities of (a) 0.05 mA cm^{-2}, (b) 0.2 mA cm^{-2}, (c) 0.5 mA cm^{-2}.

3.2. Electrochemical performance of NP-CeO_2

Fig. 3 shows the catalytic effect of NP-CeO_2 on the discharge performance of Lithium-air batteries at various current densities. The discharge voltage and capacity of the batteries catalyzed by NP-CeO_2 are improved when comparing with the ones without a catalyst. As shown in Fig. 3a, the cathode catalyzed by NP-CeO_2 delivers an initial discharge capacity of 2128 mAh g^{-1}, while 971 mAh g^{-1} for the cathode without a catalyst when discharging at 0.05 mA cm^{-2}. Clearly, the battery with NP-CeO_2 as a catalyst shows a capacity more than twice that of the one without a catalyst. The discharge voltage plateau of NP-CeO_2 catalyzed cathode is about 2.60 V, which is nearly 0.1 V higher than that of no catalyst cathode. The capacity and voltage difference indicate the electro-catalytic activity of NP-CeO_2. In general, there is a rapid decrease in the discharge capacity at a higher discharge rate. When lithium-air batteries are discharging at a constant current density of 0.2 and 0.5 mA cm^{-2}, the discharge capacity of NP-CeO_2 catalyzed cathode decreases sharply to 677 and 345 mAh g^{-1}, respectively. While the cathode without a catalyst shows a capacity of 528 mAh g^{-1} at 0.2 mA cm^{-2}, 248 mAh g^{-1} at 0.5 mA cm^{-2}.

When discharging, products of ORR deposit on the air side of the cathode. The rapid build-up of lithium oxides covers the active sites for ORR. Meanwhile, the deposits on the surface hinder the oxygen diffusion, which lead to the aggravation of polarization. The reason why CeO_2 has an advantage in decreasing polarization may be ascribed to its easy shift between reduced and oxidized states, which enable itself to play as a “ oxygen buffer ”.

It was reported that the superoxide species (O_2^-) were mainly generated on Ce^{4+} while the peroxide species (O_2^{2-}) were formed on a pair of surface cerium ions with lower oxidation state [24, 25]. After all, both superoxide species and peroxide species were involved in ORR processes [26]. It is hypothesized that the chemical processes catalyzed by CeO_2 are based on the following mechanistic steps:

$$nCeO_x\ (x<2,\ n>1) + O_2 \rightarrow [nCeO_x]^+O_2^- \rightarrow [nCeO_x]^{2+}O_2^{2-} \qquad (2)$$

$$Li^+ + O_2^- \rightarrow 2LiO_2 \qquad (3)$$

$$2Li^+ + O_2^{2-} \rightarrow Li_2O_2 \qquad (4)$$

Owing to its ability to release and uptake oxygen rapidly, it could provide relatively sufficient oxygen when discharging, which doubtlessly leads to less polarization and higher capacity.

The above tests were processed in a dry and pure oxygen glove box (RH ≤ 10%). However, the Lithium-air batteries are expected to be operated in the air (where the oxygen partial pressure is only 0.21 atm). Read et al. reported that the capacity of lithium-air batteries at 0.21 atm was only about one-fifth of those obtained in a pure oxygen environment [27]. Therefore, it is critical to emphasize the performance of lithium-air batteries in the air.

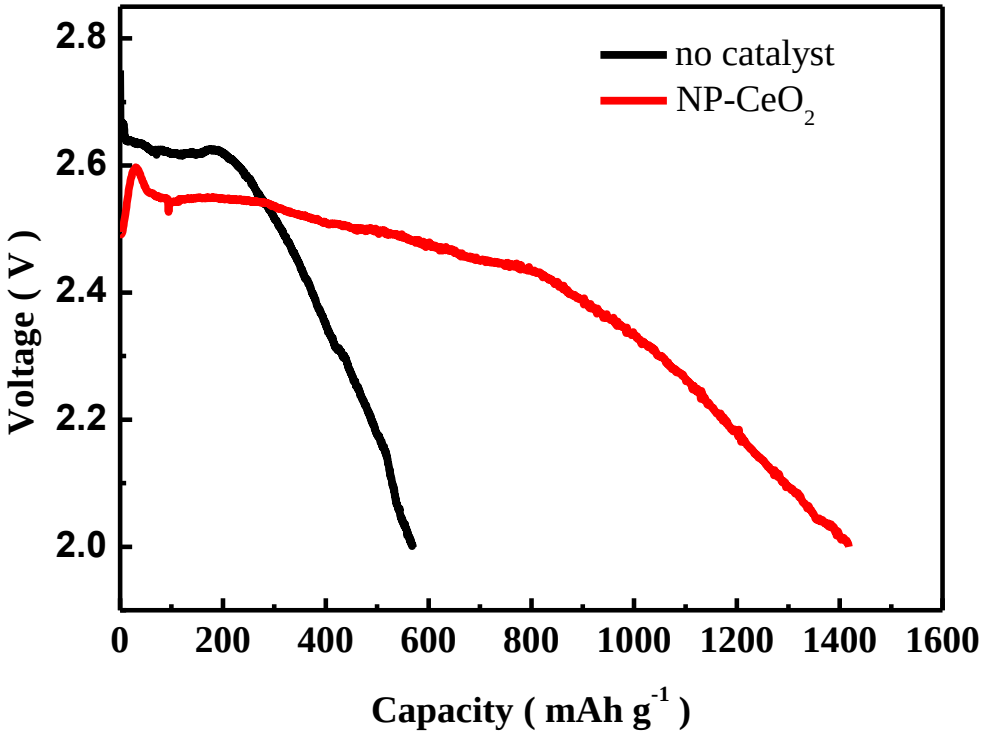

Figure 4. Discharge characteristic of lithium-air batteries in the ambient air at a current density of 0.05 mA cm^{-2}.

Fig. 4 shows the discharge curves of the cathodes catalyzed by NP-CeO_2 in the ambient air under the room temperature (RH ≈ 65%). Due to its redox properties, NP-CeO_2 catalyzed cathode delivers a much higher capacity of 1418 mAh g^{-1}, while 569 mAh g^{-1} for the cathode without a catalyst when discharging at 0.05 mA cm^{-2}. It is also found in the early stage, the discharge voltage plateau of the cathode without a catalyst is slightly higher than that of NP-CeO_2 catalyst. The reason may lay in the poor electronic conductivity of CeO_2, which may increase the polarization at some extent. However, the discharge voltage plateau of the no catalyst cathode decreases drastically and results in the end of the electrochemical reaction.

3.3. Electrochemical performance of CeO_2 with different morphologies

In order to investigate the morphology effect on the electrochemical performance [5, 28], CeO_2 of different morphologies were synthesized. Fig. 1 presents the XRD diagrams of the obtained cerium oxide catalysts with their responding crystal structures without any impurities. The XRD patterns of O-CeO_2 indicate well-defined reflections, which means the formation of crystalline structure. The SEM and TEM observations in Fig. 2b-f show that the O-CeO_2 sample is composed of regular octahedra with sharp facets and edges, the diameters of which in the range of 150-500 nm. Unlike NP-CeO_2, the S-CeO_2 are mainly composed of spherical particles. The particles agglomerate together to form large spherical particles with diameters in the range of 150–300 nm.

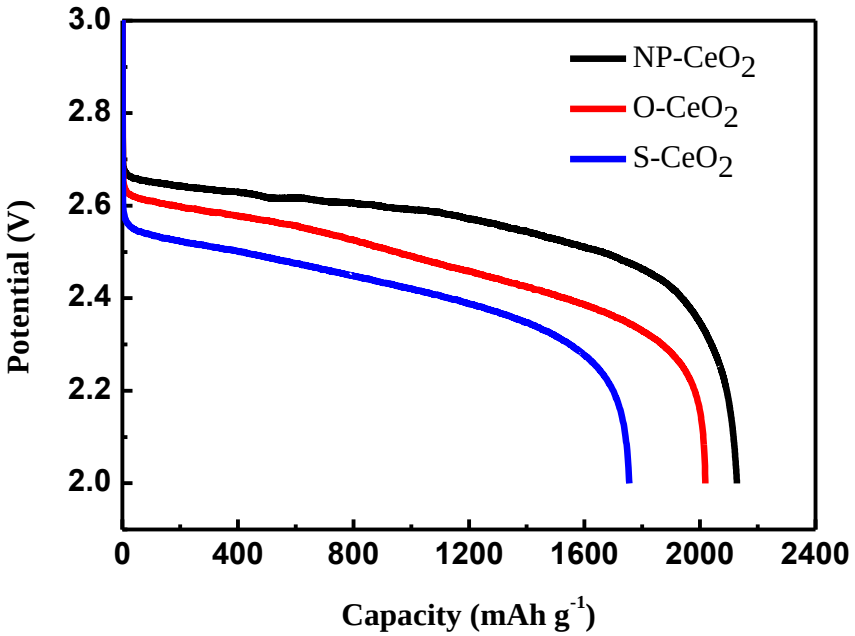

Figure 5. Discharge characteristic of lithium-air batteries catalyzed by cerium oxides at the current densities of 0.05 mA cm^{-2}.

The initial discharge curves of lithium-air batteries catalyzed by ceria in oxygen atmosphere at a current density of 0.05 mA cm^{-2} are depicted in Fig. 5. As is shown, NP-CeO_2 catalyzed battery exhibits superior initial discharge performance, delivering a discharge capacity of 2128 mAh g^{-1}. This reasonable performance is ascribed to its higher surface area of 63.1 m^2 g^{-1}, which provide more active sites for ORR reaction. However, O-CeO_2 with a surface area of 18.1 m^2 g^{-1} delivers a higher capacity of 2019 mAh g^{-1}, while 1755 mAh g^{-1} for the S-CeO_2 with a higher surface area of 39.8 m^2 g^{-1}. This observation may be connected to the specific morphology of O-CeO_2, which has affected the discharge performance in some way. It is no doubt that not only surface area but also crystal structure of cerium oxides play a great role on their electrocatalytic performance in lithium-air batteries.

4. CONCLUSIONS

CeO_2 of different morphologies were synthesized by coprecipitation and hydrothermal method, respectively. Due to its quick storing and releasing oxygen, it could play as “oxygen buffer”. By use of CeO_2 catalyst, the ORR processes in a more fluent way. This change increases the ORR rate and therefore reduces the polarization. The discharge potential of lithium-air battery using CeO_2 as the cathodes catalyst shows nearly 0.1 V higher than that of cathodes without catalyst at a current density of 0.05 mA cm^{-2}. Along with the higher operating voltage, it displays higher capacity of 2128 mAh g^{-1}, which is more than twice that of the ones without catalyst. Even when discharged in the ambient air, it still delivers a capacity of 1418 mAh g^{-1}.

The morphology effect on the discharging performance is further investigated. NP-CeO_2 with the highest surface area of 63.1 m^2 g^{-1} exhibit superior capacity. Not only surface area but also the crystal structure of cerium oxides play a great role on their electro-catalytic performance in lithium-air batteries. As is shown, CeO_2 octahedra with the lower surface area delivers the higher capacity of 2019 mAh g^{-1}, while 1755 mAh g^{-1} for CeO_2 sphere swith the surface area of 39.8 m^2 g^{-1}.

ACKNOWLEDGEMENTS
This research was financially supported by the Natural Science Foundation of China (20873032) and the Science & Technology Commission of Shanghai Municipality (08DZ2270500).

References

1. K.M. Abraham, Z. Jiang, *J. Electrochem. Soc*. 143 (1996) 1.
2. P.G. Bruce, *Solid State Ionics* 179 (2008) 752.
3. M. Armand, J.M. Tarascon, *Nature* 451 (2008) 652.T
4. [4] T. Ogasawara, A. Débart, M. Holfazel, P. Novak, P.G. Bruce, *J. Am. Chem. Soc*. 128 (2006) 1390.
5. A. Débart, A.J. Paterson, J. Bao, P.G. Bruce, *Angew. Chem. Int*. Ed. 47 (2008) 4521.
6. A.K. Thapa, T. Ishihara, *J. Power Sources* 196 (2011) 7016.
7. S. Ida, A.K. Thapa, Y. Hidaka, Y. Okamoto, M. Matsuka, H. Hagiwara, T. Ishihara, *J. Power Sources* 203 (2012) 159.
8. L. Jin, L.P. Xu, C. Morein, C.H. Chen, M. Lai, S. Dharmarathna, A. Dobley, S.L. Suib, *Adv. Funct. Mater.*, 20 (2010) 3373.
9. J.X. Lin, N. Wang, Y.H. Ding, L.H. Guan, *Electrochem. Commun*., 13 (2011) 698.
10. Y.C. Lu, Z.C. Xu, A. Gasteiger, S. Chen, H.S. Kimberly, S.H. Yang, *J. Am. Chem. Soc*. 132 (2010) 12170.
11. Y.M. Cui, Z.Y. Wen, Y. Liu, *Energe Environ. Sci.*, 4 (2011) 4727.
12. S.M. Dong, X. Chen, K.J. Zhang, L. Gu, L.X. Zhang, X.H. Zhou, L.F. Lin, Z.H. Liu, P.X. Han, H.X. Xu, J.H. Yao, C.J. Zhang, X.Y. Zhang, C.Q. Shang, G.Q. Shang, G.L. Cui, L.Q. Chen, *Chem. Commun*., 47 (2011) 11291.
13. H.L. Wang, Y. Yang, Y.Y. Liang, G.Y. Zheng, Y.G. Lin, Y. Cui, H.J. Dai, *Energy Environ. Sci*., 5 (2012) 7931.
14. L. Wang, X. Zhao, Y.H. Lu, M.W. Xu, D.W. Zhang, R.S. Ruoff, K.J. Stevenson, J.B. Goodenough, *J. Electrochm. Soc.*, 158 (2011) A1379.
15. G.Q. Zhang, M. Hendrickson, E.J. Plichta, M. Au, J.P. Zheng, *J. Electrochem. Soc*., 159 (2012) A310.
16. Z.H. Fu, X.J. Lin, T. Huang, A.S. Yu, *J. Solid State Electrochem*., 16 (2012) 1447.
17. H. Wang, X.Z. Liao, Q.Z. Jiang, X.W. Yang, Y.S. He, Z.F. Ma, *Chin. Sci. Bull*., 57 (2012) 1959.
18. J. Read, *J. Electrochem. Soc*. 149 (2002) A1190.
19. J. Read, K. Mutolo, M. Ervin, W. Behl, J. Wolfenstine, A. Driedger, D. Foster, *J. Electrochem. Soc.* 150 (2003) A1351.
20. S.S. Zhang, D. Foster, J. Read, *J. Power Sources* 195 (2010) 1235.
21. A.I.Y. Tok, F.Y.C. Boey, Z. Dong, X.L. Sun, *J. Mater. Process. Technol*. 190 (2007) 217.
22. S. Colussi, C.D. Leitenburg, G. Dolcetti, A. Trovarelli, *J. Alloys Compd.* 374 (2004) 387.
23. Y.N. Ou, G.R. Li, J.H. Liang, Z.P. Feng, Y.X. Tong, *J. Phys. Chem*. C 114 (2010) 13509.
24. E. Abi-aad, R. Bechara, J. Grimblot, A. Aboukaiss, *Chem. Mater*. 5 (1993) 793.
25. C. Li, K. Domen, K. Maruya, T. Onishi, *J. Am. Chem. Soc.* 111 (1989) 7683.

26. S. A. Freunberger, Y.H. Chen, Z.Q. Peng, J.M. Griffin, L.J. Hardwick, F. Bardé, P. Novák, P.G. Bruce. *J. Am. Chem. Soc*. 133 (2011) 8040.
27. J. Read, K. Mutolo, M. Ervin, W. Behl, J. Wolfenstine, A. Driedger, D. Foster, *J. Electrochem. Soc*., 150 (2003) A1351.
28. O. Oloniyo, S. Kumar, K. Scott, *J. Electron. Mater.*, 41 (2012) 921.

© 2012 by ESG (www.electrochemsci.org)